

EFFECT OF IMPACT LOCATION ON THE PUNCHING SHEAR RESISTANCE OF A CONCRETE WALL: NUMERICAL ANALYSES OF IMPACT TESTS USING WINFRITH AND RHT CONCRETE MODEL

Christian Heckötter¹, Jens Arndt²

¹ Technical Expert, Gesellschaft für Anlagen und Reaktorsicherheit (GRS) gGmbH, Cologne, Germany (christian.heckoetter@grs.de)

² Technical Expert, Gesellschaft für Anlagen und Reaktorsicherheit (GRS) gGmbH, Cologne, Germany

ABSTRACT

One failure mode of reinforced concrete (rc) structures subjected to concentrated impact loading is punching failure. The dynamic punching strength of a rc-slab may be estimated according to formulas given by CEB (1988) or RCC-CW (2021), which do not consider possible effects of force transmission into supports known from static loading cases. A first experimental study on these effects for impact loading was performed in the frame of the joint research project IMPACT at Technical Research Centre of Finland VTT. One reference test X4 deals with punching failure of a simply supported two-way rc-slab subjected to semi-hard missile impact. Test NEX was performed on a complex rc-mock-up, at which the loaded area is closer to supporting conditions realised by two side walls connected to the impacted front wall. Perforation occurred in X4, while the punching capacity of the front wall in NEX was not exceeded. This paper reports on numerical simulations of these experiments using LS-DYNA LSTC (2021). It is found that the Winfrith concrete material model by Broadhouse and Attwood (1993) is capable to reproduce the response of the mock-up in NEX regarding failure mode, displacements and supporting forces. Analyses on perforation should be complemented by simulations with constitutive models considering damage, e. g. the RHT concrete model by Borrvall and Riedel (2011).

INTRODUCTION

The international joint research project IMPACT is carried out at Technical Research Centre of Finland (VTT). One goal of this project is to provide test data to be used for the validation of numerical tools utilized in aircraft impact assessment.

Within this project a test program called X-series on combined bending and punching failure of reinforced concrete slabs subjected to soft missile impact has been performed. An overview on the X-series is given by Borgerhoff et al. (2022). In test X4 a simply supported two-way rc-slab (thickness 250 mm, span-width 2 m) is perforated by the missile. Formulas taken from CEB (1988) and RCC-CW (2021) for the calculation of ultimate punching capacity were applied by Darraba et al. (2022) to X-series tests. It is concluded, that pronounced slab damage must be expected for test X4. Based on application of formulas it is also concluded by Saarenheimo et al. (2015), that the ultimate punching capacity is exceeded in X4 and perforation has to be expected. However, these formulas do not consider the effect of near edge impact close to boundary conditions. Therefore, more recently a test NEX with a rc-mock-up was carried out. In this test loading, thickness and reinforcement layout of the impacted wall resemble X4, but the supporting condition deviates. Test NEX is described in detail by Vepsä et al. (2024).

This paper describes numerical simulations on X4 and NEX and the capability of the models to reproduce the different failure modes. For NEX numerical results regarding reaction forces, displacements and reinforcement strains are compared with test data.

NUMERICAL MODELLING

Tests NEX and X4 are simulated by means of explicit Finite Element (FE) method using LS-DYNA software (LSTC (2021)). An overview on the numerical model of test NEX including model components and basic measurements is given in Figure 1. The front wall is supported by its connection with the side wall. Further, its lower edge is connected to a heavy bottom slab. Due to some offset of the formwork during the casting of concrete the thickness of the front wall is larger than the targeted value of 250 mm. This is considered in the numerical model by an increase of the front face concrete cover by 20 mm. An average element size of 15 mm was chosen for hexahedral volume elements representing concrete and beam elements representing reinforcement. Every single reinforcement element is considered in the numerical set-up. Bending reinforcement density of $8.7 \text{ cm}^2/\text{m}$ is realised by bars (B500B, $\text{Ø}10 \text{ mm}$, c/c 90 mm, each way and each face), while shear reinforcement density for the front wall of $17.45 \text{ cm}^2/\text{m}^2$ is realised by closed shaped stirrups (B500B, $\text{Ø}6 \text{ mm}$, c/c360/180 mm staggered). Due to the complexity of the geometry, coupling of concrete and reinforcement is modelled by means of a constraint condition rather than by shared nodes. Further shear reinforcement elements are included in the side walls and in the bottom slab at locations of the vertical supports. A simplified version of the Johnson-Cook (1983) model according to Equation 1 is used to simulate material behaviour of reinforcement, at which values of $A=512 \text{ MPa}$, $B=663 \text{ MPa}$, $n=0.533$, $C=0.025$ and reference strain rate of $\dot{\epsilon}_0 = 10^{-8} \text{ s}^{-1}$ are used. A failure criterion of 10% effective plastic strain is assumed.

$$\sigma_y = (A + B \cdot \epsilon_p^n) \cdot (1 + C \cdot \ln \frac{\dot{\epsilon}_p}{\dot{\epsilon}_0}) \quad (1)$$

Horizontal support against the laboratory wall is realised by explicitly modelling the four back pipes ($\text{Ø}=125 \text{ mm}$, $t=12.5 \text{ mm}$) using shell elements and a contact condition between steel plates and side walls. Nodes of steel plates at the laboratory wall are fixed. For the vertical fixation of the mock-up to the ground floor the identical system is used as for the IRIS-3 test campaign, which was subject of an OECD Nuclear Energy Agency benchmark activity (see NEA (2023)). An existing model (see Heckötter (2022)) shown in Figure 2 is used for vertical fixations. Due to the pre-stressed spotweld-elements representing the anchors this model allows vertical uplift of the mock-up as well as horizontal deflections of the lower anchor plate. Effects of gravity were minor in trial calculations and are neglected.

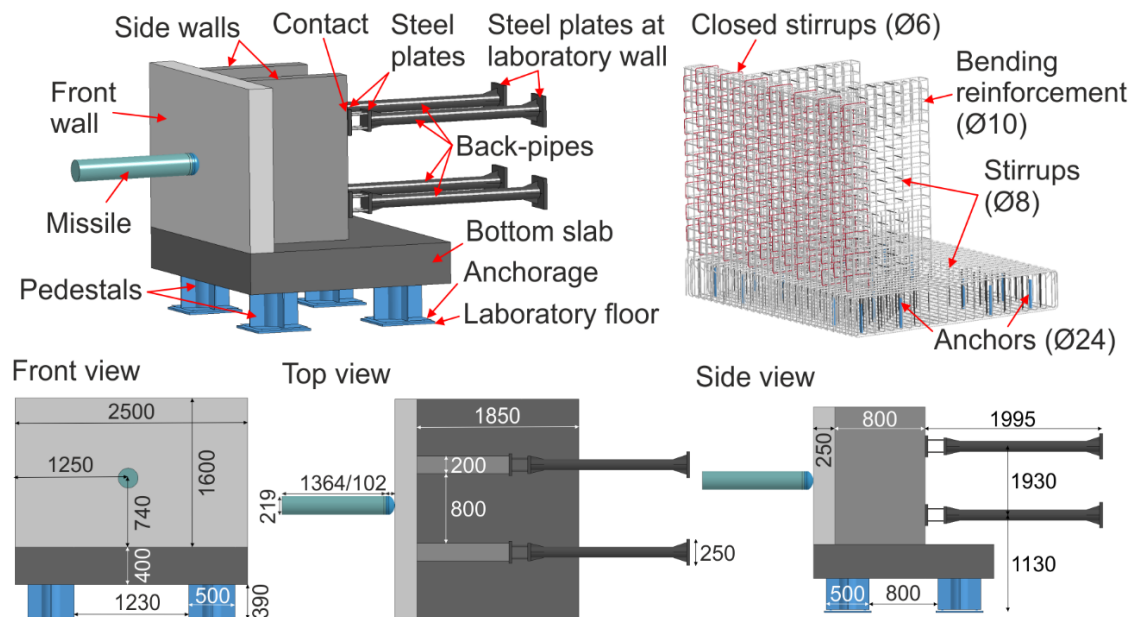


Figure 1. Numerical model for LS-DYNA of test NEX including basic measurements (in mm).

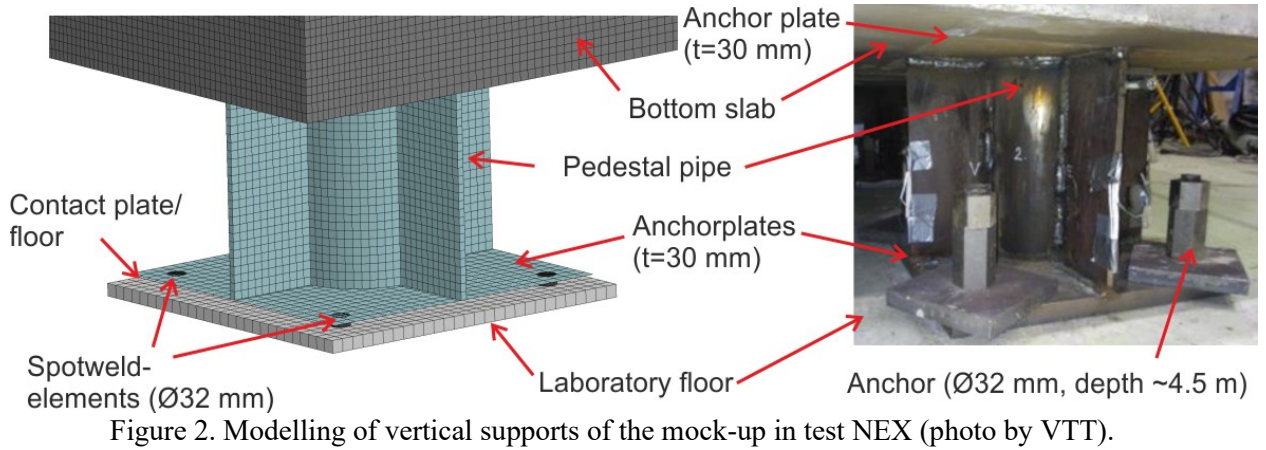


Figure 2. Modelling of vertical supports of the mock-up in test NEX (photo by VTT).

The deformable missile made of stainless steel (EN 1.4432) with a total mass of ca. 50 kg is composed of a tube (outer diameter 219 mm, thickness 6.35 mm) and a spherical nose cap (length 102 mm, thickness 3.76 mm) which are each fitted and welded to a steel band (length 50 mm, thickness 4 mm). It is represented by fully integrated shell elements with a relatively fine average mesh size of 4.5 mm to capture the folding mechanism. Material behaviour is considered by a piecewise linear plasticity model using a stress-strain relationship provided by VTT (see Figure 3). Strain rate effects are considered according to the dynamic increase factor (DIF) of the Cowper-Symonds (1957) form given in Equation 2 for the dynamic yield stress σ_{dyn} , in which the model parameter D corresponds to the strain rate that doubles the static yield stress σ_{stat} . For selected parameter sets for D and q the variation of DIF with strain rate is shown in Figure 3. According to Jones (1989) the average strain rate during the folding of the missile might be estimated by $\dot{\epsilon} \approx \frac{v_0}{4R}$, which gives a value of about 390 s^{-1} for an impact velocity of $v_0=165.8 \text{ m/s}$ and $r=106 \text{ mm}$. The effect of strain rate on stress-strain relationship for $D=100 \text{ s}^{-1}$ and $q=10$ is also shown in Figure 3.

$$\sigma_{dyn} = \sigma_{stat} \cdot \left(1 + \left[\frac{\dot{\epsilon}}{D} \right]^{1/q} \right) = \sigma_{stat} \cdot DIF \quad (2)$$

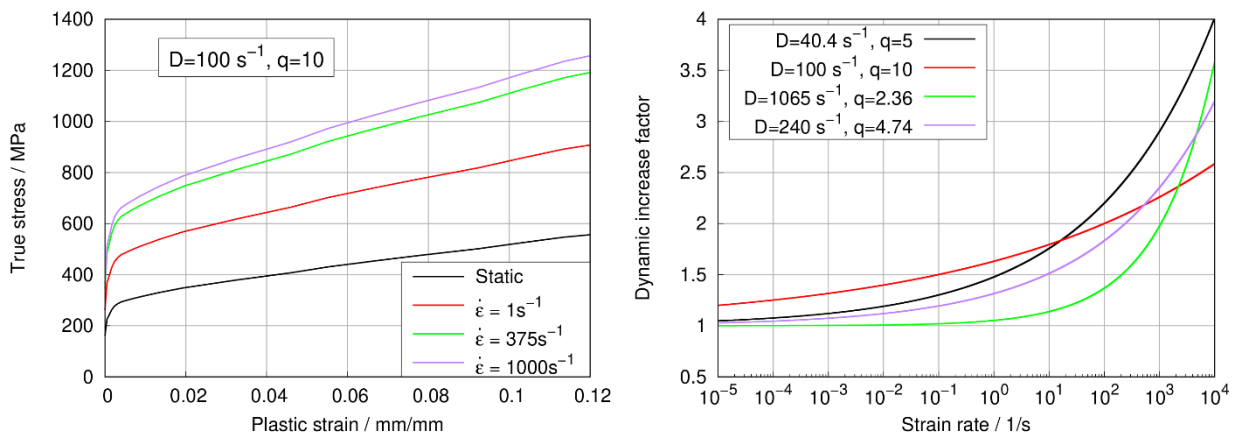


Figure 3. Stress-strain relations for EN 1.4432 stainless steel and DIF of Cowper-Symonds model.

Concrete material behaviour is described by the Winfrith model (Broadhouse and Attwood (1993)) considering strain rate effects and input parameters of 2.33 g/cm^3 for density, 31.87 GPa for Young's modulus, 0.197 for Poisson's ratio, 52.1 MPa for cubic compressive strength, 3.64 MPa for tensile strength, 148.7 J/m for fracture energy and 4 mm for the maximum aggregate radius. The Winfrith model is well suited to simulate bending failure including formation of plastic hinges in reinforcement (see Heckötter (2022)), but material damage including reduction of elastic constants is not considered. Therefore, additional simulations using the RHT model in LS-DYNA (Borrvall and

Riedel (2011)) were carried out to analyse possible effects of material damage, especially on possible perforation of the slab.

NUMERICAL RESULTS

Figure 4 compares missile deformations of tests X4 and NEX with simulation results. In test NEX ($v_0=165.8$ m/s) splitting of the missile pipe and separation of the cap was observed. Further, some buckling of the pipe with three folds occurred. In test X4 ($v_0=168.6$ m/s) mainly buckling of the missile pipe with four on-axisymmetric folds was observed, while the cap was crushed into the pipe. Some minor splitting of the pipe is also visible. In numerical simulations fracture effects are not considered and axisymmetric buckling occurs, at which the number of folds depends on the choice of Cowper-Symonds parameters. It should be mentioned that neglecting strain rate effects results in an unrealistic large number of folds and consequently an overestimation of deformed length.

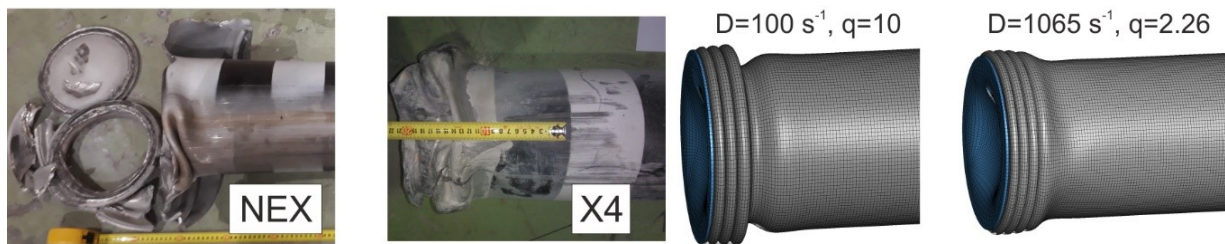


Figure 4. Deformed missiles in tests NEX and X4 compared with numerical results (photos by VTT).

Low-pass filtered numerical contact forces for different assumptions on Cowper-Symonds parameters are shown in Figure 5. Despite the choice of $D=1065$ s⁻¹ and $q=2.26$ the effect on peak impact forces is relatively low. No effect on momentum transfer can be observed, which is due to rebound slightly larger than the initial momentum of the missile. Trial calculations on NEX showed, that displacements revealed just a small dependency on the Cowper-Symonds parameters. Since three folds were observed in test NEX, values of $D=100$ s⁻¹ and $q=10$ given by Nordberg (2004) for stainless steel are used in this study. However, due to the splitting of the missiles some uncertainty on the loading remains. By trend the splitting is expected to reduce the average impact forces. Neglecting the splitting results in an overestimation of loading and target damage and is therefore considered to be a conservative approach.

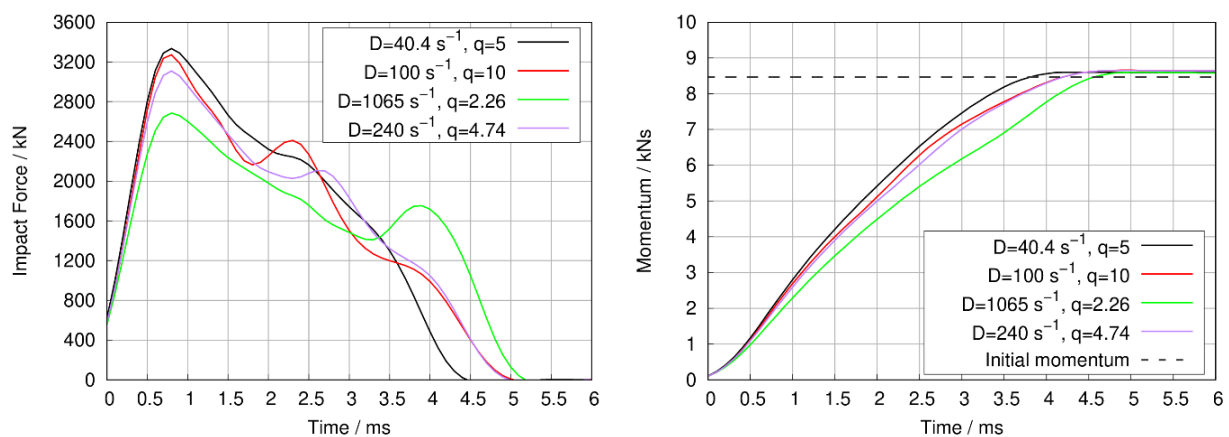


Figure 5. Numerical contact forces (left) and momentum transfer for loading in test NEX.

Perforation of the slab with residual velocity of about 25 m/s occurred in test X4. Damage states of the section are compared in Figure 5 to numerical results, using the crack visualization option of the Winfrith model and contour plots of the damage parameter of the RHT model. Originally the RHT model was implemented in AUTODYN and later in LS-DYNA (see Borrvall and Riedel (2011)). Figure 6 presents results of an accomplished code comparison. The failure criterion of reinforcement is

exceeded for several elements. In simulations using the Winfrith model an element erosion criterion of 40% effective strain is used, which enables separation of the punching cone and perforation of the missile with a finite residual velocity. It turned out, that this erosion criterion reproduces the failure mode of NEX, too. However, the failure mode and residual missile velocity generally may depend on the erosion criterion, which is not physically based. Due to this drawback, it is not possible to generalise predictions of a failure mode to other scenarios. Therefore, additional calculations using the RHT concrete model were performed with two analysis codes. The RHT model considers material damage and residual strength of crushed concrete, at which erosion is only used to avoid termination of the calculation due to small explicit time steps. Consequently, a time-step based erosion criterion is used, which does not affect prediction of a specific failure mode. It correctly reproduces the different failure modes for X4 and NEX. On the other hand, specification of input parameters may be difficult. In particular this applies for parameters describing residual strength of totally crushed concrete (see Heckötter and Sievers 2022).

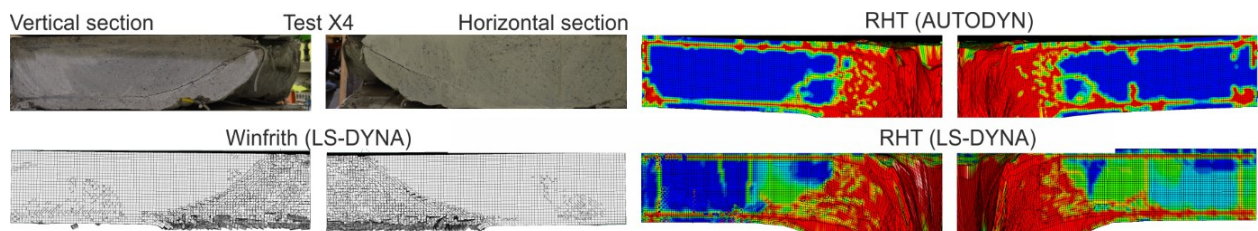


Figure 6. Comparison of cross section damage in test X4 (photos by VTT).

In contrast to X4 no perforation occurred in test NEX, which is reproduced by the Winfrith model as well as by the RHT model. The failure criterion of reinforcement is not exceeded by any element. Crack patterns calculated with the Winfrith model are compared to test results in Figure 7. Close to the connection of front wall and bottom slab some cracks occurred in the test, which are not observed in numerical simulations. Formation of a punching cone in the front wall is apparent from the section. The punching angle is satisfyingly reproduced by the simulation.

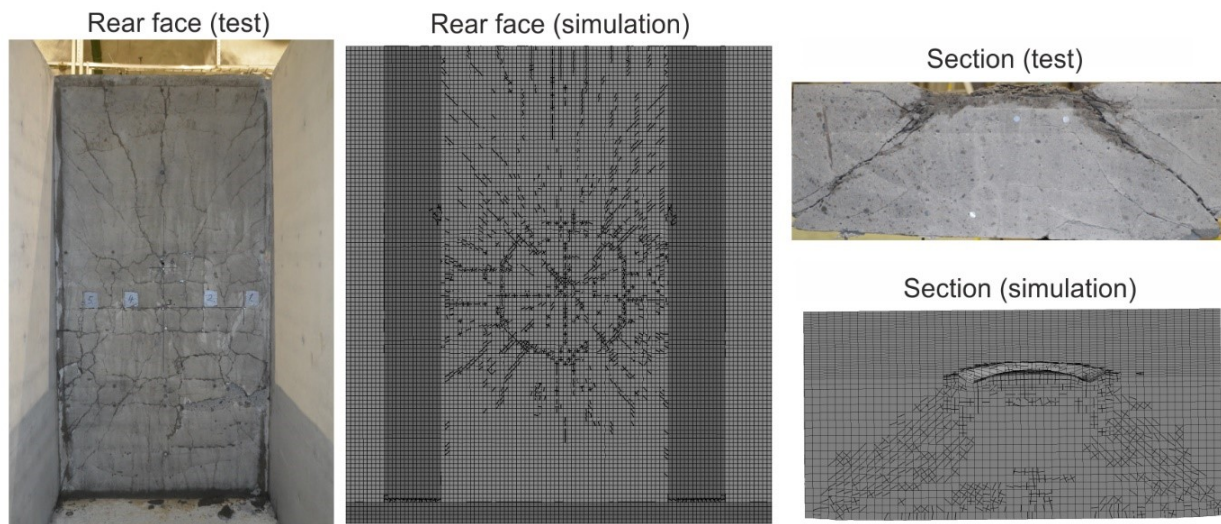


Figure 7. Crack patterns on rear face and in the section of the front wall in test NEX (photos by VTT).

Measured and calculated reaction forces are compared in Figure 8. Low-pass filtered contact forces between side walls and steel plates (see Figure 1) are associated with numerical results for horizontal reaction forces, while coupling forces between bottom slab and pedestal pipes (see Figure 2) are associated with vertical reaction forces. A pronounced asymmetry is visible in test data on horizontal forces, which in this extent is not reproduced by the simulation. Especially the calculated upper contact forces overestimate measured horizontal peak forces, while the widths of peaks are underestimated. Further, secondary contacts occur with deviating frequency and intensity. All the differences mentioned

above are attributed to the representation of vertical fixations. As expected, during the initial phase of the impact test tensile forces are observed in front vertical supports, while compression occurs at rear vertical supports. During the post-impact vibration major differences occur regarding peak forces and frequencies. Further, differences between left- and right-hand side of rear pedestals are not covered by the simulations. Sensitivity studies revealed that back pipe stiffness has minor effects on frequencies and horizontal forces. However, a less detailed modelling of vertical supports yields even less realistic results. In simulations of IRIS-3 tests the detailed model of the fixation yielded good results regarding vertical forces. A mayor difference between IRIS-3 tests and NEX is the loading. Calculated peak impact forces of IRIS-3 tests are 400 kN and 900 kN (see Heckötter (2022)) are significantly lower than in test NEX (see Figure 5) with values above 3 MN. Right now, there is no workaround for an improved representation of modelled boundary conditions. The correct representation of nonlinear pull-out behaviour of anchors in vertical direction out of the laboratory floor seems to be a major challenge for the modelling.

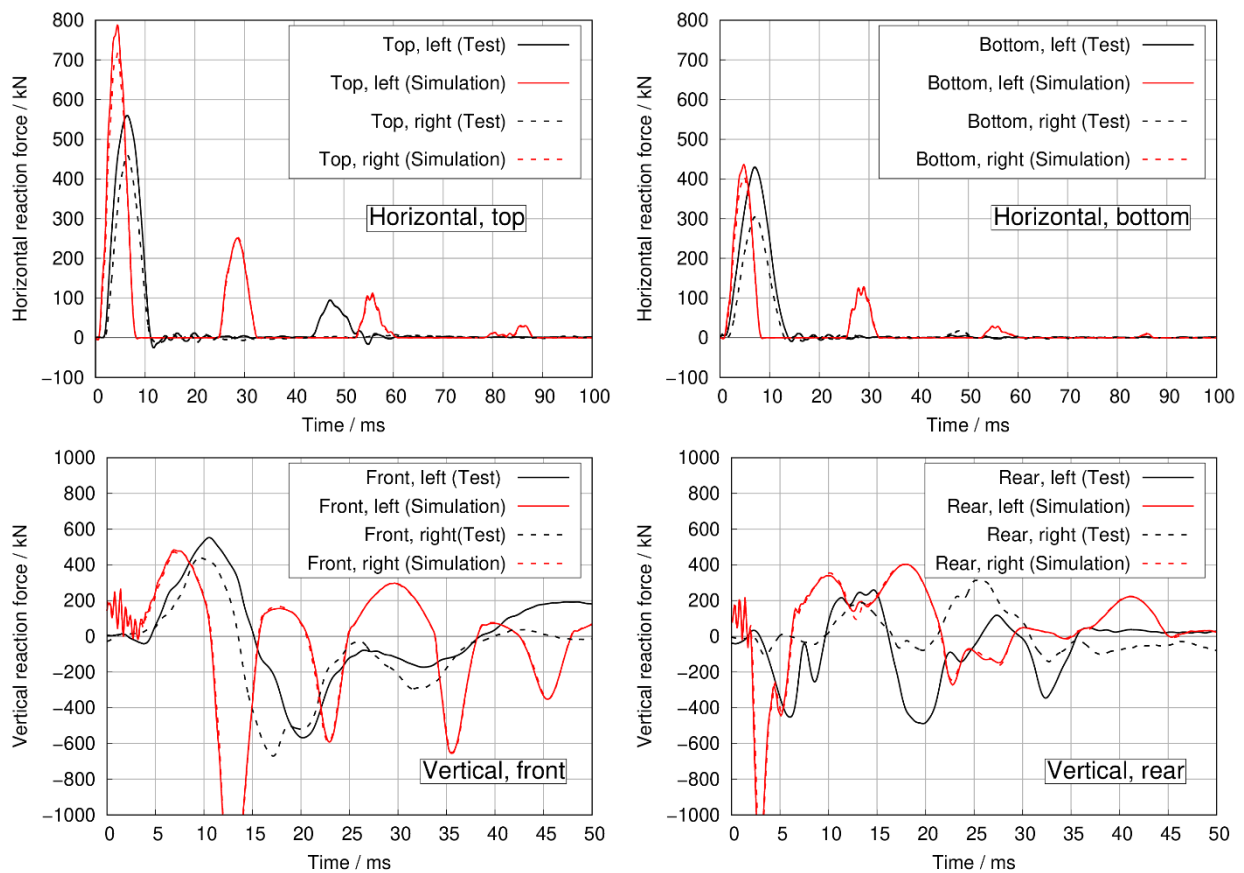


Figure 8. Comparison of calculated and measured horizontal and vertical reaction forces for test NEX.

Figure 9 compares horizontal momentum transfer to the supports on the left- and right-hand side as well as the total momentum with the initial momentum of the missile. Apparently, the momentum transfer derived from test data is larger on the left-hand side, which is consistent with the direction of impact point offset from the centre. This effect is less pronounced in the numerical results. The total momentum transfer derived from the first contact is similar for simulation and test data. Presumably due to inertia of the mock-up and rebound of the missile these values are larger than the initial momentum of the missile.

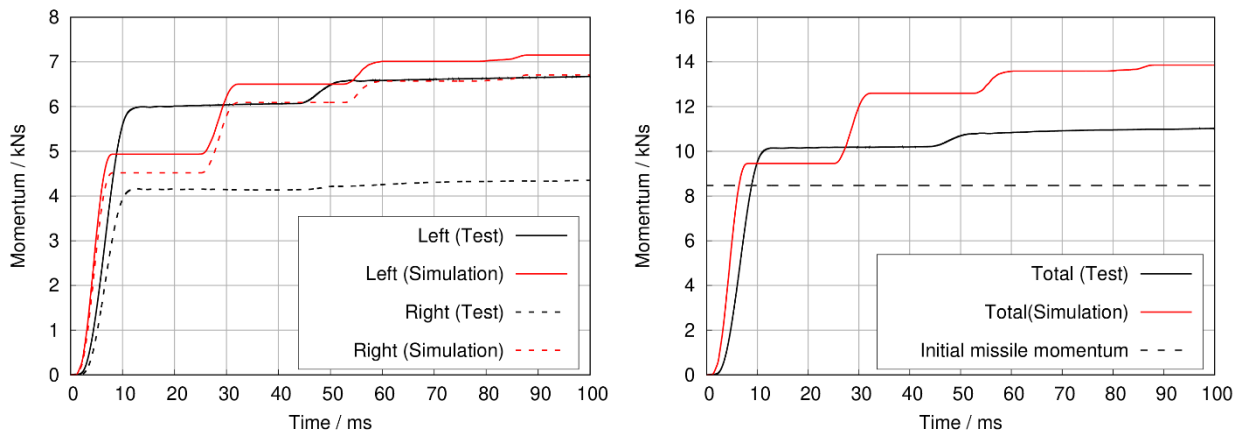


Figure 9. Measured and calculated momentum transfer to horizontal supports in test NEX.

The mock-up is instrumented with displacement transducers attached to the rear face of the front wall, rear face of the bottom slab and centre of the side walls. Displacements are measured parallel to the direction of impact at locations of D1-D6 and D9/D10 and in lateral direction at locations of D7/D8. Strains of front wall reinforcement are measured by strain gauges glued on front face bars (B1-B6), rear face bars (B11-B13) and stirrups (S2). Figure 10 shows a front view of the instrumentation layout.

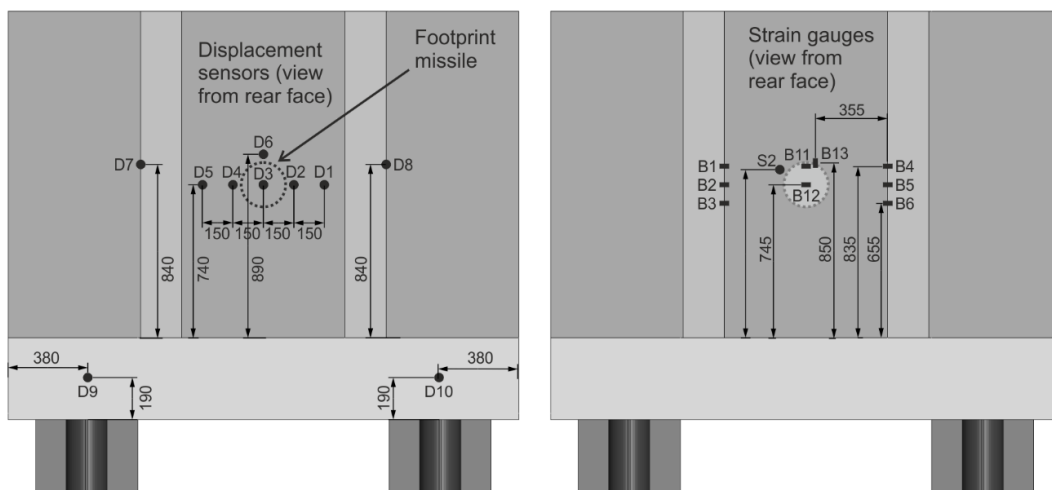


Figure 10. Locations of displacement sensors and reinforcement strain gauges in test NEX (in mm).

Measured and calculated displacements are compared in Figure 11. The offset of the impact point of about 35 mm toward sensor D2 observed in the test is considered in the model. Thus, at locations D1 and D2 somewhat larger maximum displacements are observed than at locations of D4 and D5. This applies also for permanent deflections displayed in the displacement figure. Since differences for maximum values among D1-D6 are quite small, it can be concluded that the bending deflection between the side walls is relatively limited. Differences between results of simulation and test data regarding post impact vibration frequency are attributed to deficits concerning the representation of vertical supports. The horizontal response of the mock-up is considered as too stiff in simulations. A simplified modelling of vertical supports results in even larger post-impact vibration frequencies. The increase of concrete cover by 20 mm has some effect on maximum displacements. Neglecting this increase results in about 15% higher displacements. On the other hand, Cowper-Symonds parameter of $D=1065 \text{ s}^{-1}$ and $q=2.26$ results in about 15% lower displacements. Displacements at locations of D9/D10 are small and results are quite symmetric. Lateral displacements at locations of D7/D8 are symmetric, but test data of D8 seems questionable after 20 ms.

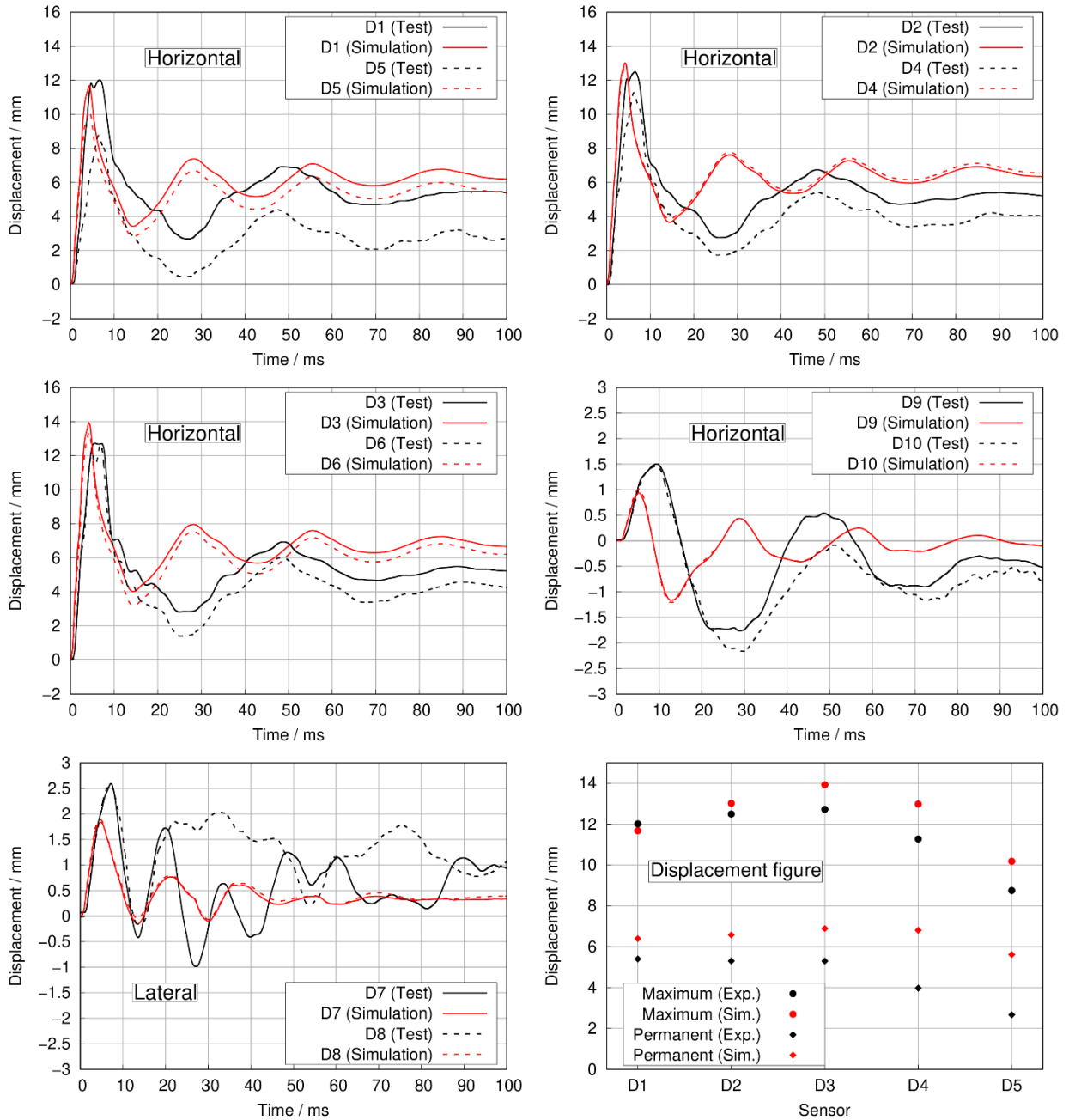


Figure 11. Comparison of calculated and measured displacements for test NEX.

Results on reinforcement strains are compared in Figure 12. In some cases, test data and simulation results agree reasonably well. For some sensors (e. g. B1) an interpretation of simulation results is difficult due to permanent strains in compression. The largest reinforcement strains in the model as well as in the test are observed in rear face reinforcement at the centre of the impacted front wall. Test data are quite different for horizontal (B11) and vertical (B13) bars. This difference is not observed in the numerical results, even though maximum displacements are well determined. The differences may be attributed to local effects such as concrete cracking or buckling of reinforcement bars, which are not necessarily reproduced by numerical simulations. Measurements at S2 located on a stirrup in the region of the punching cone are well captured by the simulation. Some plastic deformation of S2 can be observed.

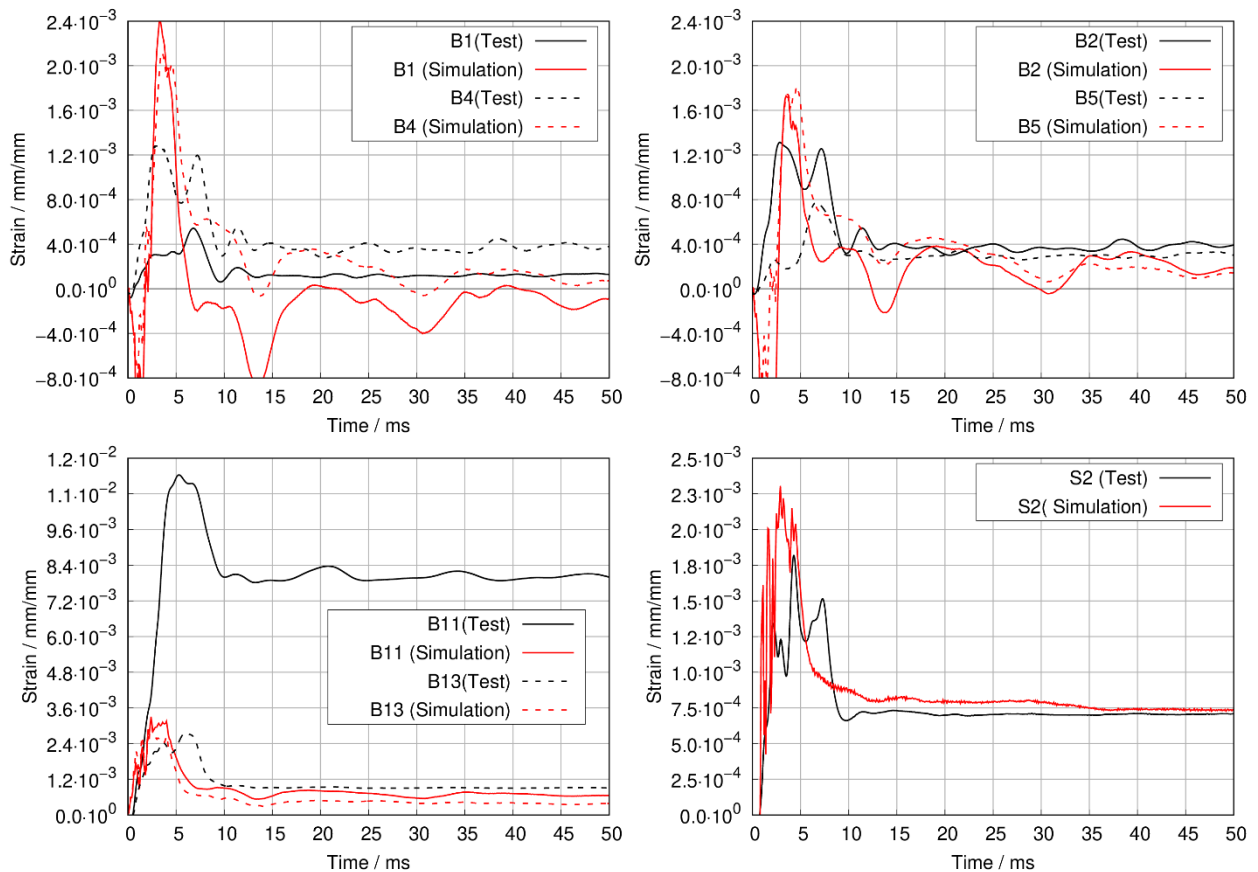


Figure 12. Comparison of calculated and measured reinforcement strains for test NEX.

CONCLUSION

The effect on failure mode of an impact near a supporting condition found in impact test NEX is reproduced by numerical simulations and compared with test X4. Regarding crack patterns of concrete as well as maximum and permanent displacements of the front wall the Winfrith concrete model yields satisfying results in simulations of test NEX. Regarding frequencies of front wall displacements during post impact vibrations differences occur between test data and simulation results. Further differences include post impact vibrations of horizontal support forces, vertical reaction forces and level of asymmetry of the results. These differences are attributed to deficits in the description of vertical fixation. Modelling of the connection between mock-up and laboratory floor is supposed to be more challenging for test NEX than in the IRIS test campaign, since impact forces are larger in NEX. An improvement of the model would require a realistic representation of the vertical pull-out behaviour of anchor bars.

Compared to displacements reinforcement strains seem to be more difficult to simulate and simulation results only partly agree well with test data. This is presumably due to local effects such as concrete cracking and local buckling of reinforcement bars.

In addition to buckling some splitting of the missile occurred in test NEX, which is supposed to affect the load time function. Currently the splitting mechanism is not covered by numerical simulations, which may give rise to some deficits regarding representation of loading.

Possible perforation of the structure should be investigated in additional simulations using a concrete material model considering damage (e. g. the RHT model). Using the Winfrith model and fitting an erosion criterion to match the perforation failure mode observed in one particular test is questionable, because the erosion criterion is not physically based and transferability of the model to other impact scenarios cannot be ensured.

ACKNOWLEDGEMENT

The work was carried out in the frame of the German reactor safety research program funded by the Federal Ministry for the Environment, Nature Conservation, Nuclear Safety and Consumer Protection (BMUV).

REFERENCES

- CEB (1988). *Concrete Structures Under Impact and Impulsive Loading*, Bulletin D'Information No. 187, Comite Euro-International du Beton.
- Borgerhoff, M. et al. "Interaction of Bending and Punching in Reinforced Concrete Slabs Subjected to Impacts of Deformable Projectiles in IMPACT III Project Tests," In *SMiRT-26*, Potsdam/Berlin, Germany.
- Borrvall, T., Riedel, W. (2011). "The RHT Concrete Model in LS-DYNA," In *8th European LS-DYNA Conference*, Strasbourg, France.
- Broadhouse, B.J., Attwood, G.J. (1993). "Finite Element Analysis of the Impact Response of Reinforced Concrete Structures using DYNA3D," In *SMiRT-12*, Stuttgart, Germany.
- Cowper, G. R., Symonds. P. S. (1957). *Strain-hardening and strain-rate effects in the impact loading of cantilever beams*, Division of Applied Mathematics, Brown University, USA.
- Darraba, A. et al. (2022). "Verification of Punching Damage of Reinforced Concrete Slabs under Soft Impact with RCC-CW Punching Resistance," In *SMiRT-26*, Potsdam/Berlin, Germany.
- Heckötter, C. (2022). "Numerical Simulation of Experiments on Impact Induced Vibrations – Comparison of IRIS Phase 3 and IMPACT V3 Mock-Ups with Respect to Boundary Conditions," In *SMiRT-26*, Potsdam/Berlin, Germany.
- Heckötter, C., Sievers, J. (2022). "Punching Failure of Reinforced Concrete Slabs Subjected to Hard Missile Impact, Part III: Simulation of Recent Tests With the RHT-Model in LS-DYNA," In *SMiRT-26*, Potsdam/Berlin, Germany.
- Johnson, R. J., Cook, W. H. (1983). "Constitutive Model and Data for Metals Subjected to Large Strains, Strain Rates and High Temperatures," In *7th Int. Symposium on Ballistics*, The Hague, Netherlands.
- Jones, N. (1989). *Structural Impact*, Cambridge University Press.
- LSTC (2021). *LS-DYNA, A Program for Nonlinear Dynamic Analysis of Structures in Three Dimensions, Version R13*, Livermore Software Technology, an ANSYS Company, USA.
- NEA (2023). *IRIS Phase 3: Tests description and interpretation & Round robin calculations analysis*. OECD Nuclear Energy Agency, NEA/CSNI/R(2023)5.
- Nordberg, H. (2004). *Note on the Sensitivity of Stainless Steels to Strain Rate*. Research Report No 04.0-1, AvestaPolarit Research Foundation ad Sheffield Hallam University.
- RCC-CW (2021). *RCC-CW 2021 Edition – Rules for Design and Construction of PWR Nuclear Civil Works*, AFCEN ed.
- Saarenheimo, A. et al. (2015). "Bending and Punching Studies on Impact Loaded Plate," In *SMiRT-23*, Manchester, United Kingdom.
- Vepsä, A. et al. (2024). "The Effect of Impact Location on the Punching Shear Resistance of a Concrete Wall: Near Edge Impact Test," In *SMiRT-27*, Yokohama, Japan.